Investigation of light-matter interaction in single vertical nanowires in ordered nanowire arrays

Ziyuan Li *[a], Li Li [b], Fan Wang [c], Lei Xu [d], Qian Gao [a], Ahmed Alabadla [a], Kun Peng [a], Kaushal Vora [b], Haroldo T. Hattori [e], Hark Hoe Tan [a,f], Chennupati Jagadish [a,f], and Lan Fu *[a,f]

[a]*Department of Electronic Materials Engineering, Research School of Physics, The Australian National University, Canberra, ACT 2601, Australia. Email: ziyuan.li@anu.edu.au, lan.fu@anu.edu.au*

[b]*Australian National Fabrication Facility, Research School of Physics, The Australian National University, Canberra, ACT 2601, Australia*

[c]*School of Electrical and Data Engineering, Faculty of Engineering and Information Technology, University of Technology Sydney, Ultimo, NSW 2007, Australia*

[d]*Advanced Optics and Photonics Laboratory, Department of Engineering, School of Science & Technology, Nottingham Trent University, Nottingham, NG1 4FQ, United Kingdom*

[e]*School of Engineering and Information Technology, University of New South Wales, Canberra, ACT 2610, Australia*

[f]*Australian Research Council Centre of Excellence for Transformative Meta-Optical Systems, Research School of Physics, The Australian National University, Canberra, ACT 2601, Australia*

Abstract

Quasi one-dimensional semiconductor nanowires (NWs) in either arrays or single free-standing forms have shown unique optical properties (i.e., light absorption and emission) differently from their thin film or bulk counterparts, presenting new opportunities for achieving enhanced performance and/or functionalities for optoelectronic device applications. However, there is still a lack of understanding of the absorption properties of vertically standing single NWs within an array environment with light coupling from neighboring NWs within certain distances, due to the challenges in fabrication of such devices. In this article, we present a new approach to fabricate single vertically standing NW photodetectors from ordered InP NW arrays using the focused ion beam technique, to allow direct measurements of optical and electrical properties of single NWs standing in an array. The light-matter interaction and photodetector performance are investigated using both experimental and theoretical methods. The consistent photocurrent and simulated absorption mapping results reveal that the light absorption and thus photoresponse of single NWs are strongly affected by the NW array geometry and related light coupling from their surrounding dielectric environment, due to the large absorption cross section and/or strong light interaction. While the highest light concentration factor (~ 19.64) was obtained

from the NW in an array with a pitch of 1.5 μm, the higher responsivity per unit cell (equivalent to NW array responsivity) of a single vertical NW photodetector was achieved in an array with a pitch of 0.8 μm, highlighting the importance of array design for practical applications. The insight from our study can provide important guidance to evaluate and optimize the device design of NW arrays for a wide range of optoelectronic device applications.

Keywords: InP, single vertical nanowire, light-matter interaction, photodetector, focused-ion beam

Introduction

III-V compound semiconductor nanowire (NW) arrays have attracted significant attention for optoelectronic device applications such as light-emitting diodes,[1-3] lasers,[4, 5] solar cells,[6-8] photodetectors,[9-12] as well as biological detectors and sensors.[13-15] Their unique one-dimensional morphology and associated optical and electrical properties lead to interesting nanophotonic effects that are not presented in their planar counterparts,[16, 17] as well as more efficient strain relaxation making it easier for incorporation of heterostrutures and/or growth on different substrates such as Si for on-chip photonic integration.[18-20] In particular, vertically-aligned NW arrays have low reflection and strong broadband absorption, which could be used as both an active and antireflection layer to couple light into high index semiconductors more efficiently.[21, 22] In addition, NW arrays may reduce the amount of material usage to reduce cost while produce more functional devices.[23-25] Among different III-V NW materials, InP is particularly promising for optoelectronic applications due to its direct bandgap and very low surface recombination velocity (161 cm/s),[26, 27] with ideal electronic band gap energy of 1.344 eV for near-infrared photodetectors and solar cell applications.[22]

Light-matter interaction in both NW arrays and a single NW have been investigated both theoretically and experimentally, demonstrating distinctly different light absorption properties from their thin film or bulk counterparts leading to enhanced performance[28-30] and/or functionalities[27, 31, 32] for photodetector or solar cell applications. It is well known that for a single NW lying horizontally on a substrate, light

absorption along the NW axis is uniform,[33-35] whereas vertical NWs exhibit position-dependent light absorption profile.[36] Different resonance modes would also be supported in NWs that have different configurations, such as whispering gallery modes or leaky modes in horizontal NWs and conventional waveguide modes in vertical NWs.[37] For example, for vertical NWs, Krogstrup *et al.* reported a single standing NW solar cell with an apparent efficiency (defined by the current density from the NW physical cross-section) of 40%.[28] The reason for such high efficiency is the mismatch between the absorption cross-section and the physical bounds of the NW, indicating an unexpectedly large absorption cross-section and thus a high built-in light concentration of the vertical NW geometry. By using well-developed numerical simulation methods, it is also revealed that the optical response in NWs is dominated by diffraction of light due to their diameter that is comparable to the wavelength of light.[38-40] It means that the light that travels adjacent to a single NW or between NWs could also be absorbed by NWs[40] as demonstrated by absorption measurements.[28, 41] Therefore, in the case of NW arrays, constructive interference and thus competition for photon absorption within NWs exist but diminish when the separation between NWs increases.[39, 40] A direct quantitative comparison of absorption in laterally and vertically oriented core-shell InP NW p-i-n solar cell has been performed by a joint experimental-theoretical method, revealing that the array pitch plays a determining role.[39] Depending on the pitch, absorption in a vertical NW in an array could be lower than, equal to, or higher than that in a horizontal single NW with the same dimensions.[39] It is also important to consider that increasing the NW array pitch size would decrease the number of NWs per unit area, and subsequently reduce the overall solar cell or photodetector performance.[39] All these investigations indicate that the design guidelines for enhancing the light absorption in a device cannot be directly transferred from a single (horizontal) NW to an NW array.[40] On the other hand, while there are a few limited experimental studies on single vertical NWs in an ordered NW array, such as the optical absorption using fluorescence confocal microscopy[42] and the electrical behavior contacted by a tungsten

nano-probe,[43, 44] no experimental work has been reported to directly investigate their light-matter interaction effect with different array pitch size, and the corresponding photodetector performance.

In this work, the focused ion beam (FIB) technique was employed to fabricate single vertical NW photodetector devices from an ordered NW array, allowing for the direct characterization as well as the comparison with the simulations of their light absorption and photocurrent generation properties. The photocurrent maps of the single vertical NW devices in arrays were measured and simulated, demonstrating a significantly larger absorption cross-section than their physical cross-section. Consequently, a larger light concentration effect with the increase of array pitch is observed until it can be treated as an isolated single NW. However, while small array pitch size would constrain the NW absorption cross-section, the coupling between adjacent NWs in the array can localize light more effectively within the NWs, leading to an optimum pitch size with an overall higher absorption than NWs with larger pitch size (equivalent to a single free standing NW) and thus higher detector performance (i.e., responsivity and detectivity). Our work provides a new method to not only study the fundamental light-matter interaction property of single vertical NWs, but also evaluation of their device performance, which will be important for the design and optimization of NW array-based optoelectronic devices.

Methods

Nanowire synthesis: High-quality stacking fault-free and taper-free wurtzite (WZ) InP NWs were grown in a metalorganic vapor phase epitaxy (MOVPE) reactor (AIXTRON 200/4) using the selective-area growth technique[26, 27, 33] as measured by transmission electron microscopy reported in Reference [26]. Firstly, a 30 nm SiO_2 mask layer was deposited on a (111)A n-type InP substrate by a plasma-enhanced chemical vapor deposition system. Electron beam lithography and buffered hydrogen fluoride etching were then used to create hexagonal arrays of nanoscale circular holes in the oxide with a diameter of ~ 200 nm and an array pitch of 0.8, 1.5 and 2.2 μm. The NWs were grown at 730 °C for 5 min with

trimethylindium and PH_3 as the precursors at a flow rate of 6.1×10^{-6} and 4.9×10^{-4} mol/min, respectively, corresponding to a group V/III ratio of ~ 80. After MOVPE growth, the NW morphology was characterized using scanning electron microscopy (SEM). An optical characterization setup including a micro-photoluminescence (μ-PL) spectroscopy and a time-correlated single-photon counting system was employed to assess the NW optical quality. A 522 nm solid-state pulsed laser with a pulse width of 300 fs, repetition rate of 20.8 MHz and beam diameter of ~ 610 nm through a 100× objective lens (NA 0.9) was used as the excitation source for PL, time-resolved PL and power-dependent PL of single NWs lying on a SiO_2 (300 nm)-on-Si substrate at room temperature in air. Under this laser repetition rate, 1 mW average laser power equals to an excitation pulse energy of 48 pJ. In order to avoid band filling and band gap renormalization effects, low excitation powers of 0.025−2.45 μW (corresponding to < 0.2 pJ/pulse) were used.

Single nanowire photodetector fabrication: A promoter (AP3000) layer was first spun onto the as-grown sample at 4000 rpm for 30 s followed by several drops of benzocyclobutene (BCB) onto the surface as the planarization layer. After 5 min settlement, the sample was spun at 4000 rpm for 1 min and baked on a hot plate at 100 °C for 2 min. Then a vacuum oven was employed to hard bake the sample, with the temperature ramping up from 100 to 250 °C, dwelling at 250 °C for 60 min and ramping down to 20 °C. After all these steps, a dual-beam FIB system (FEI Helios 600 NanoLab) equipped with a Ga^+ ion beam was used to etch back the BCB layer, so that the tips of the NWs were exposed. In this work, an ion beam current of 28 pA was applied to slowly etch away the BCB at a selective area in NW arrays to expose the tip of only one NW. The area size can be adjusted based on the NW diameter and array pitch, i.e., 0.8×0.8 μm^2 for array pitch of 0.8 and 1.5 μm, and 1×1 μm^2 for array pitch of 2.2 μm. After FIB etching, wet chemical etching with 9% HCl for 1.5 min was conducted to remove the surface oxide, followed by the deposition of a 500 nm-thick indium tin oxide (ITO) layer as transparent contact using a sputter coater

system. Finally, Ti/Au contact (10 nm/200 nm) was deposited on the back side and selected area of the top ITO layer using an electron beam evaporator.

Characterization Method: The generated photocurrent from single vertical NWs was evaluated by photocurrent maps measured by a WITec alpha300S scanning microscopy system, where the light at 532 nm from a Fianium WhiteLase supercontinuum laser was focused by a 100× NA 0.9 objective lens with a spot diameter of ~ 721 nm, and scanned across the sample using a piezo-driven sample stage. The spectral response of the single NW detectors was measured under the illumination of a tungsten-halogen lamp as a white light source with a spot size of 11 μm in diameter through an Acton SpectraPro® 2300i monochromator. In both systems, the photocurrent was measured using the conventional amplitude modulation technique employing a digital generator or mechanical chopper at a frequency of 333 Hz, a Stanford SR570 low-noise current pre-amplifier and a Stanford SR850 digital lock-in amplifier.

Results and discussion

Figures 1 (a)-(c) show the top and (d)-(f) 30° tilted SEM images of the InP NW array grown on a SiO_2 patterned InP substrate with an opening hole diameter of 200 nm and a pitch of p = 0.8, 1.5 and 2.2 μm, respectively. Although all NWs are taper-free and stacking fault-free WZ crystal structures, their morphology varies with pitch size. The NWs from the array with a pitch of 0.8 μm have mostly regular hexagonal cross-sections and are uniform in side-to-side diameter (~ 230 nm) and length (~ 2.6 μm). The NWs from the array with a pitch of 1.5 μm have irregular and larger hexagonal cross-sections and less uniformity in diameter (280-330 nm) and length (3-3.6 μm). The NWs from the array with a pitch of 2.2 μm have the most irregular hexagonal or triangular cross-sections and large variation in diameter (280-640 nm) and length (2.3-3.8 μm). This is due to the increase of collection area around the openings of SiO_2 layer with increasing pitch, which allows more adatoms to diffuse towards the NWs to contribute to the lateral growth and cause increased irregularity and non-uniformity.[26, 34, 45] Nevertheless, such

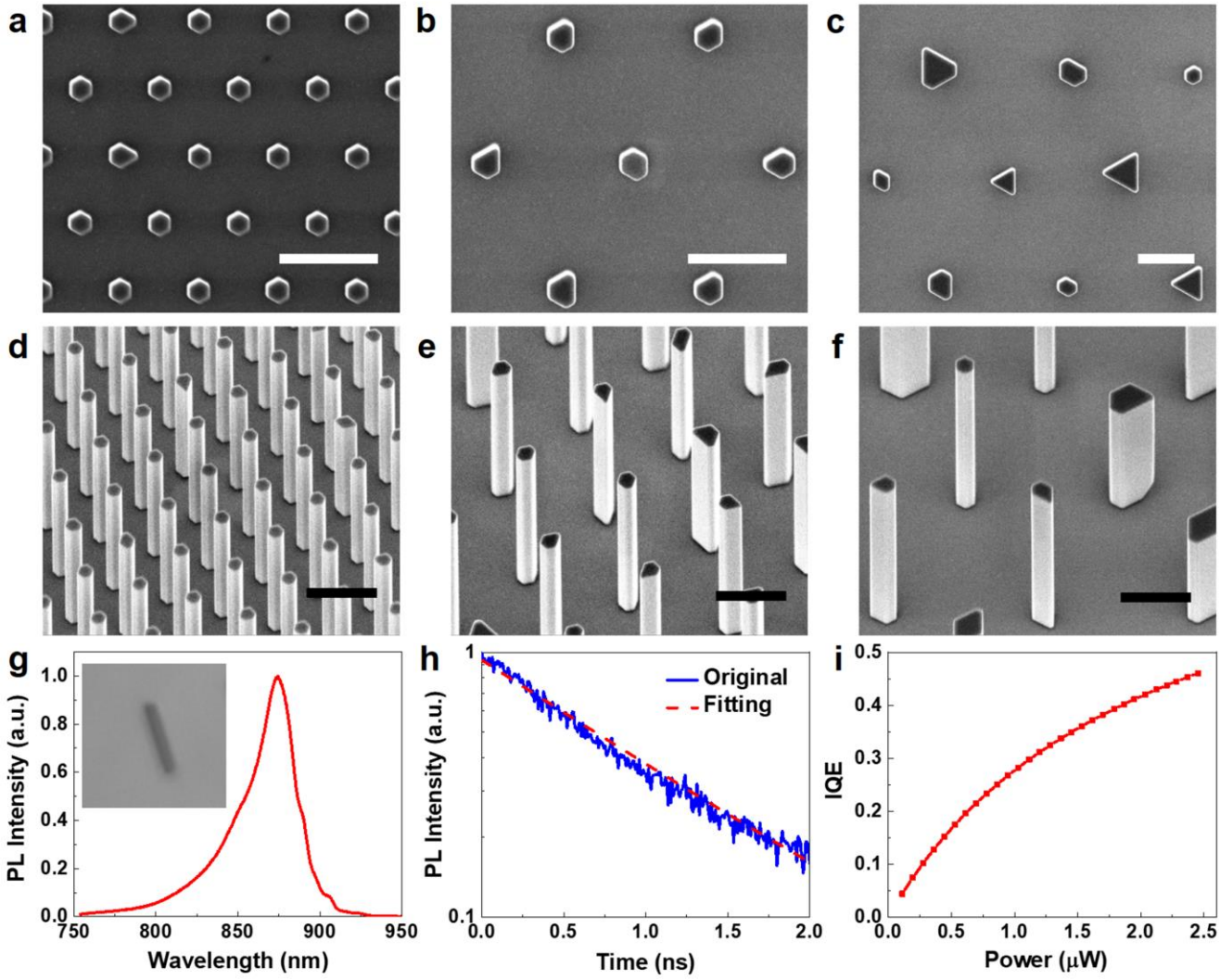

Figure 1. (a)-(c) Top and (d)-(f) 30° tilted view SEM images of as-grown InP NW arrays with p = 0.8, 1.5, 2.2 μm, respectively. The scale bars are 1 μm. (g) Normalized PL spectrum of a single horizontal NW at room temperature. The inset shows the optical image of the NW. (h) PL intensity decay of the NW is fitted by a single exponential decay with lifetime of 1.1 ns. (i) Power-dependent IQE extracted from the fits of the carrier rate equation.

morphology change does not adversely affect the optical properties of the NWs. Figure 1 (g) shows the room temperature PL measurements of a single horizontal InP NW transferred from an array with a pitch of 2.2 μm. The NW exhibits a strong peak emission wavelength at around 874 nm (1.42 eV) which can be attributed to the band edge emission from WZ InP.[26] The time-resolved PL intensity decay of such NW can be fitted by a single exponential decay with a lifetime of 1.1 ns, as presented in Figure 1 (h). The power-dependent internal quantum efficiency (IQE) (Figure 1 (i)) is also a quantitative factor reflecting the NW optical quality, which was extracted from the fitting of the carrier rate equation based on the

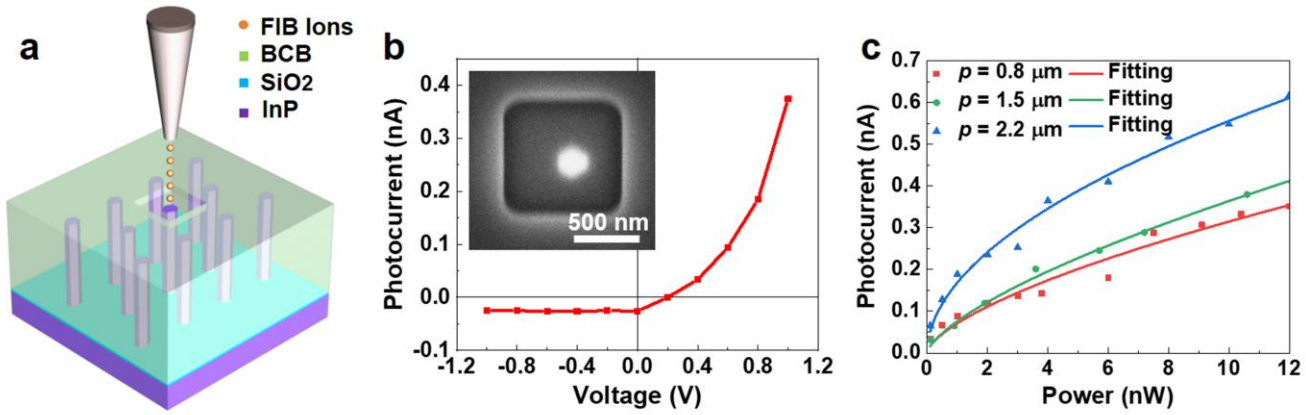

Figure 2. (a) Schematic of a single vertical NW device by FIB etching. (b) Photocurrent of a single vertical NW photodetector versus bias voltage, where a positive bias voltage applied on top of the NW is defined as a forward bias voltage. The inset shows an SEM image of such single NW in the array with p = 0.8 μm. (c) Photocurrent versus power with fitted curve of such NW based photodetector from the array with p = 0.8, 1.5 and 2.2 μm, respectively, under the laser illumination at wavelength of 532 nm.

power-dependent PL measurement.[33] A statistical investigation of the detailed PL study of NWs from all three arrays is provided in Figure S1. The long minority carrier lifetimes (~ 1 ns) and high IQE (up to 50%) obtained from the three NW samples indicate their excellent optical quality and suitability for optoelectronic applications.

Figure 2 (a) illustrates the schematic of the single vertical NW device fabricated by FIB etching. For each NW array, a few single NW photodetectors have been fabricated to provide statistical data. The current-voltage (*I-V*) characteristics of the single vertical NW devices after fabrication were measured in dark (Figure S2) and under laser illumination. The photocurrent is extracted from the maximum value of the photocurrent maps at different bias voltages. Under light illumination at the wavelength of λ = 532 nm, with a fixed intensity of 1224 mW/cm^2, a photocurrent exhibiting diode behavior is obtained (see Figure 2 (b)) with good photoresponse under the positive bias from the single NW photodetector. A small level of photocurrent generated at 0 V and reverse bias can also be observed, which may be due to a Schottky junction formation at the ITO-NW interface with a low barrier height. The photocurrent with an error bar of 0.38 ± 0.12 nA is obtained by extracting the photocurrent of 6 single vertical NW photodetectors in an array (p = 0.8 μm) at 1 V. Photocurrent versus power intensity of the single vertical

NW photodetector in an array with a pitch of 0.8, 1.5 and 2.2 μm under the 532 nm laser illumination is shown in Figure 2 (c), respectively. It is found that the relationship between photocurrent and input optical power can be expressed by a simple power law:[46, 47]

$$I_{ph} \propto P^{\alpha}, \quad (1)$$

where P is the excitation power and α is the power-law exponent with a fitted value of ~ 0.65, 0.68 and 0.52 for p = 0.8, 1.5 and 2.2 μm, respectively, indicating similar material quality of the NWs from these three different arrays. Such non-unity exponent is due to the complicated process of carrier generation, trapping, and recombination within the NW.[47-49]

To investigate the light-matter interaction experimentally, the photocurrent generated by the single vertical NWs in arrays of p = 0.8, 1.5 and 2.2 μm was spatially mapped, under a forward bias of 1 V. Since the shape and size of the NWs in arrays with p = 1.5 and 2.2 μm are not very uniform, relatively small and hexagonal shaped NWs were chosen from these arrays for the mapping comparison with the NW from a pitch of 0.8 μm, as shown in the insets of Figure 3 (a)-(c). The normalized scanning photocurrent maps in Figure 3 (a)-(c) were deconvoluted with the point-spread function (PSF) of the diffraction-limited spot size (a Gaussian beam with a spot size of 721 nm in diameter).[28] The detailed deconvolution process using MATLAB is explained in Figure S3, to extract the photocurrent cross-section from the single NW. The maps all show two-dimensional Gaussian-like photocurrent distributions, with highest photocurrent generated in the NW center. Compared with single NWs from arrays with p = 1.5 and 2.2 μm, the full width at half maximum (FWHM) of the peak photocurrent of the single NW from an array with p = 0.8 μm is much smaller, however a strong interaction of light with uncontacted surrounding NWs can be observed from the photocurrent map as indicated by the light blue photocurrent contrast. When the pitch is small, light absorption by the single NW interferes significantly with neighboring NWs and thus limits its effective absorption cross-section.[39] The regular shape of NWs from array p = 0.8 μm

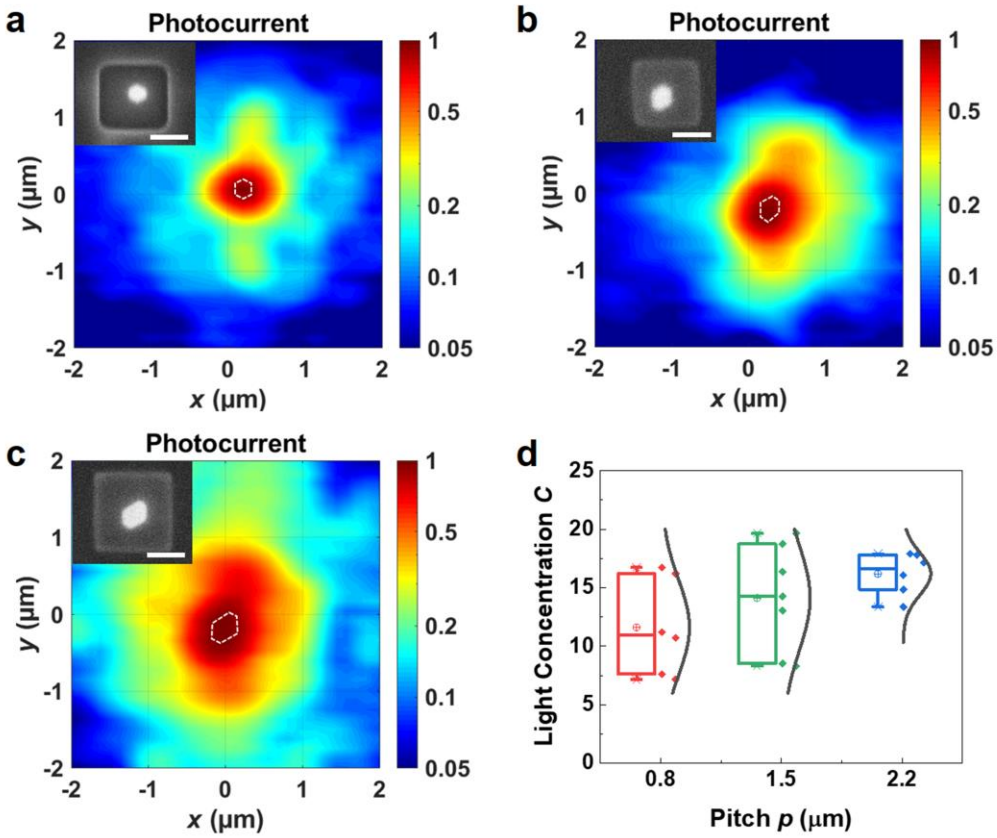

Figure 3. Normalized scanning photocurrent map with a logarithmic scale color bar of single NW from array with pitch of (a) 0.8, (b) 1.5 and (c) 2.2 μm, respectively. SEM images of as-measured NW devices are shown in the insets correspondingly. The scale bars are 500 nm. The NWs are also highlighted by white dotted outlines. (d) Light concentration (*C*) of single NW devices from arrays with p = 0.8, 1.5 and 2.2 μm, respectively.

also results in a fairly regular photocurrent cross-section. When the pitch size increases, light absorption of the single NW detector is less affected by the neighboring NWs and eventually the NW can be treated as an isolated single NW when the pitch size is large enough.[39] While there is a large area indicating non-zero photocurrent, the main photocurrent is contributed by collecting light from the open area surrounding the NW. The irregular and elongated (in the *y*-axis) shape of NWs from those arrays (p = 1.5 and 2.2 μm) also leads to irregular shapes of their photocurrent cross-sections; while their larger physical cross-section than that of p = 0.8 μm would also result in larger photocurrent cross-section. Based on the deconvoluted Gaussian-like maps, we define the area with photocurrent no less than half of the maximum photocurrent as the effective absorption cross-section $S_{abs} = S_{phys}\eta_{ab}$, where S_{phys} is the physical cross-section of the NW and η_{ab} is the absorption efficiency that is equal to a built-in light concentration C.[28] Based upon these

definitions/parameters, the absorption cross-section of the single vertical NW detector in Figure 3 from the array with p = 0.8, 1.5 and 2.2 μm is estimated to be 3.49×10^5, 6×10^5 and 1.48×10^6 nm^2, respectively, indicating a larger effective absorption cross-section than their respective physical cross-section (4.89×10^4, 7.21×10^4 and 9.23×10^4 nm^2). The built-in light concentration factors obtained from multiple NWs measured from the three NW arrays are presented in Figure 3 (d), all with a value higher than 1. The highest light concentration factor of ~ 19.64 was obtained from an NW in an array with p = 1.5 μm. However, for these three pitch sizes, they all show large variation of light concentration probably due to the variation of NW morphology, material quality and device fabrication, indicating the challenges of accurate control of NW growth and device fabrication. The average light concentration factor of the NWs from an array with p = 2.2 μm is ~ 16, which is similar to that obtained by Krogstrup *et al.* (~ 12) for a single standing GaAs NW with a diameter of 380 nm (S_{phys} = 9.38×10^4 nm^2),[28] demonstrating the vertical NWs' ability to extend its effective absorption cross-section.

To compare and further understand the experimental mapping results, 3D FullWAVE finite-difference time-domain (FDTD)[50] simulation was performed by scanning a light beam across the NW array with an area of 4×4 μm^2 to examine the absorption of the center NW in arrays with various pitch sizes. A Gaussian plane-wave source in a diameter of 721 nm was used to simulate the laser beam. The NW hexagonal cross-section was set to be the same as the size of experimentally examined NWs in Figure 3, as shown in the contour maps of Figure S4. The vertical length (l) was set to be 2.6 μm. The computational region was terminated by perfectly matched absorbing regions. The grid sizes were $\Delta x = \Delta y = \Delta z$ = 20 nm and the time step was set well below the stability limit. The absorption of the center NW was obtained by normalizing the total power absorbed within the domain of a monitor including the whole center NW by the input power. A deconvolution process has been taken with the PSF of the diffraction-limited laser spot to obtain the absorption maps as shown in Figure 4 (a)-(c). Consistent with the experimental results shown in Fig. 3, the simulated absorption map of a single NW in an array with p = 0.8 μm shows that the

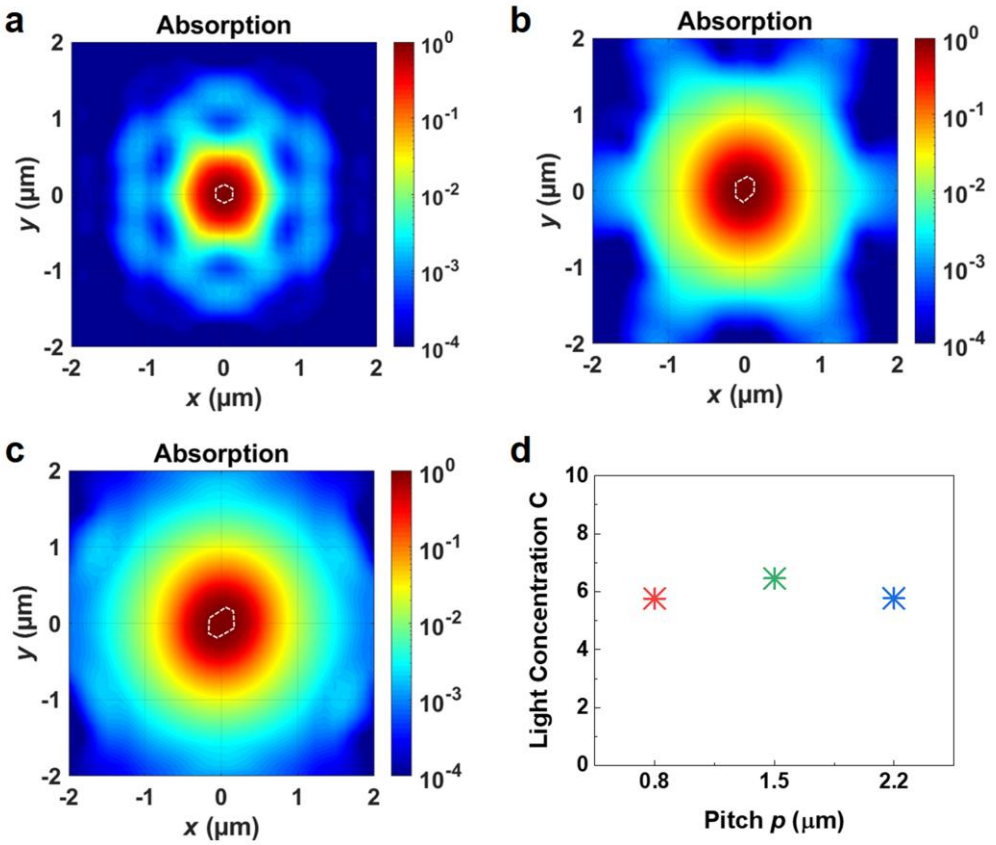

Figure 4. Simulated absorption map with a logarithmic scale color bar of single NW from array with pitch of (a) 0.8, (b) 1.5 and (c) 2.2 μm, respectively. The outline of the NWs are shown by white dotted lines. The intensity color bar is in log scale. (d) Light concentration (C) of single NW devices from arrays with p = 0.8, 1.5 and 2.2 μm, respectively. The area with absorption no less than half of the maximal photocurrent is defined as the effective absorption cross-section area.

absorption area of the center NW is rather confined within a radius of ~ 500 nm, but there are strong interactions in between NWs, leading to some light absorption area overlapping with the positions of surrounding NWs. The absorption map of a single NW from an array with p = 1.5 μm also shows some light interference with surrounding NWs but with much broader absorption cross-section; whereas the map of a single NW from an array with p = 2.2 μm exhibits almost an ideal two-dimensional Gaussian-function absorption distribution, with nearly no interference with surrounding NWs. If we define the effective absorption cross-section as the area with absorption no less than half of the maximum absorption, an effective absorption cross-section of 2×10^5, 4.66×10^5 and 1.48×10^6 nm^2 is obtained for p = 0.8, 1.5 and 2.2 μm, respectively, which is much larger than their physical cross-section (3.46×10^4, 7.21×10^4 and 9.23×10^4 nm^2). The light concentration versus array pitch size is also shown in Figure 4 (d). As can be

seen, for the simulation based on the real NW sizes, a single NW from an array with p = 1.5 μm displays the highest absorption, which is consistent with the experimental results, confirming again that both large absorption cross-section and light interaction with surrounding NWs would affect the NW absorption and thus lead to an optimal light concentration in NWs. It is noticed that despite a consistent trend, the simulated C values (Fig. 4 (c)) are smaller than the ones obtained experimentally (Fig. 3 (d)). We ascribe it to two main reasons. Firstly, as can be seen from the SEM images, the variation of individual NW shape and diameter from SAE grown NW arrays becomes increasingly significant with the increase of array pitch, which causes inevitable discrepancy between the experimental and simulated results. Secondly, due to the FIB fabrication, a small trench (shown in Fig. 2 (b) and Fig. 3) was formed around the single NW, which could lead to ineligible light scattering at the edge during photocurrent mapping causing additional absorption in NW and contribute to the photocurrent signal.

The absorptance (A) of the NWs within arrays with various pitch sizes was also simulated by setting a vertical NW in a unit cell with a plane wave of light illuminated onto the whole unit cell along the NW axis through Lumerical software. The NW length was set as 2.6 μm and side-to-side diameter d as 300 nm. In the simulations, the refractive index of zinc-blende (ZB) InP was used. Since our NWs should be placed in a hexagonal array of period/pitch p, the simulation domain is marked by the dotted red line with a width equaling to p and length equaling to $\sqrt{3}\bullet p$ using periodic boundaries as shown in Figure S6 (a), which actually contains two NWs. Therefore, the modeled absorptance is defined as the fraction of incident intensity absorbed by a vertical NW placed in the shaded hexagonal cell marked by the dark dotted line whose area is half of the simulation domain, and thus the lattice area is $S_{lattice} = \sqrt{3}\bullet p^2/2$, which actually corresponds to the absorption/photocurrent per unit cell. To give a deeper insight on the absorption properties of each NWs, we also calculated the absorption efficiency of our structure as shown in Figure 5 (b), which is defined as $(A\bullet S_{lattice}/S_{phys})$,[28, 39] the ratio between the absorption cross-section of NW in the array to its physical cross-section. It shows how much larger area than the geometrical cross-

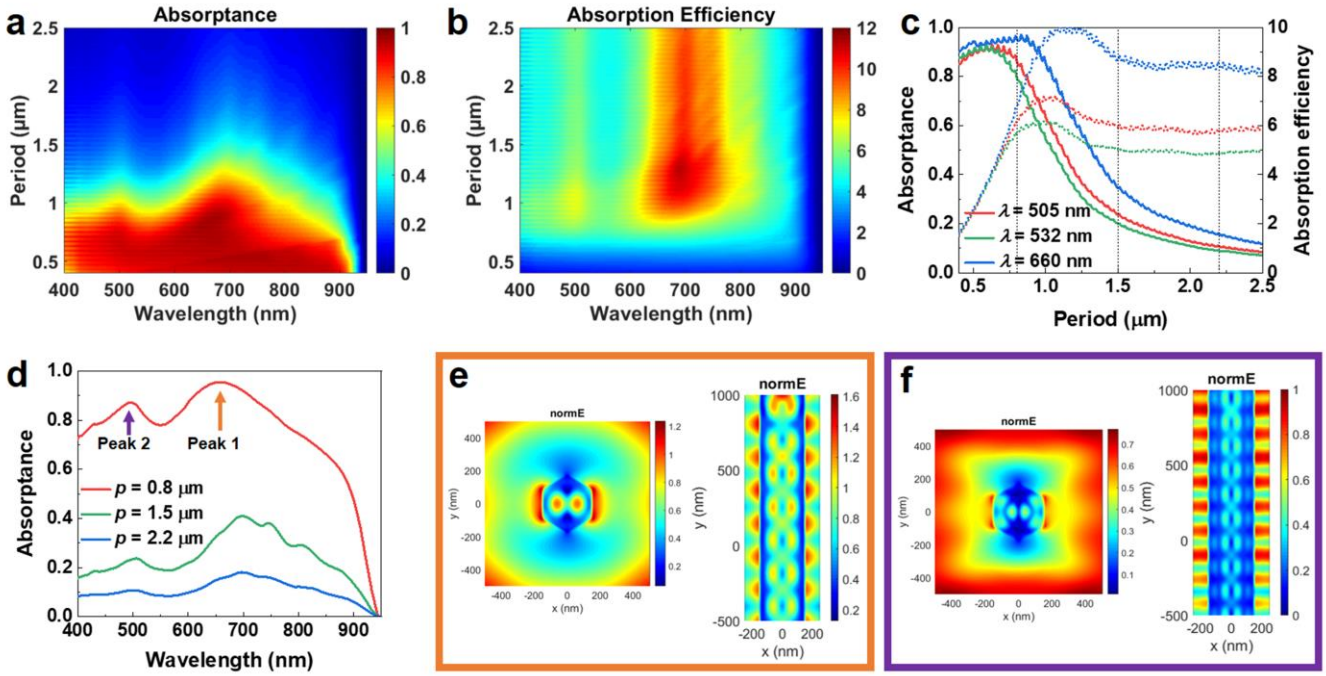

Figure 5. Simulated (a) absorptance and (c) absorption efficiency of a 2.6 μm InP NW with diameter of D = 300 nm standing in a hexagonal array of period p. (c) Absorptance (solid lines) and absorption efficiency (dotted lines) of the same nanowire at the two peak wavelength of 505 and 660 nm as well as the experimental operating wavelength of 532 nm, extracted from (a) and (b), respectively. (d) Absorptance versus wavelength for p = 0.8, 1.5 and 2.2 μm extracted from (a). Electric field distributions of the single nanowire from the array with period of 0.8 μm for (e) Peak 1 at λ = 660 nm and (f) Peak 2 at λ = 505 nm, respectively.

sectional area our NW can absorb the incident light, corresponding to the light concentration per NW in Figures 3 (d) and 4 (d). To efficiently absorb the light incident on each unit cell and maximize the absorptance of our NWs array, this absorption cross section from the individual NW of each unit cell needs to maximally cover and overlap with the unit cell. As shown in Figure 5 (c), under the illumination of a wavelength of 660 nm, the absorptance at $p \leq 0.94$ μm remains more than 90% and drops gradually when p is larger than 0.94 μm. For smaller illumination wavelengths, it shows the same trend with peak absorption at smaller pitch size. Since the absorptance considers the absorption ability per unit area, the results provide a direct implication of the current density produced by NW array detectors. As clearly shown, as the pitch size increases from 0.8 to 2.2 μm, the absorptance decreases largely, as a result of the reduced number of NWs per unit area, implying that the largest photocurrent will be generated from the array with a pitch of 0.8 μm. On the other hand, the absorption ability shows increased absorption ability

with increased *p* when it is small, then being saturated, and decreased to a constant level when the NWs can be treated as isolated single NWs. It indicates that there is an optimal trade-off between vertical configuration-introduced large absorption cross-section and strong light interaction among NWs in the array.

To obtain the optimal pitch size for the NW with this diameter, we calculated the average absorptance as shown below:

$$\overline{A} = \frac{1}{\lambda_1 - \lambda_0} \int_{\lambda_0}^{\lambda_1} A(\lambda) d\lambda, \quad (2)$$

where, λ_0 = 400 nm and λ_1 = 950 nm. As shown in Figure S6 (b), when p = 0.55 μm, the average absorptance can be as high as 88.3%. We then obtained the simulated absorption versus wavelength and NW diameter for NW array with pitch of 0.55 μm as shown in Figure S6 (c). After calculating the average absorptance for each diameter as indicated in Figure S6 (d), we found that when the diameter is larger than 180 nm, the average absorptance is all higher than 80% and reaches 88.6% when the NW diameter is 295 nm.

Furthermore, two absorption peaks at λ = 660 nm (Peak 1) and λ = 505 nm (Peak 2) can be identified in Figure 5 (d). The electric field distributions of each individual NW show that Peak 1 originates from resonant absorption through the HE_{12} waveguide modes as indicated by Figure 5 (e), while Peak 2 corresponds to the HE_{13} waveguide modes as shown in Figure 5 (f). The mode distribution also demonstrates that the large effective absorption cross-section is strongly related to the coupling of light into weakly guided modes leading to strong absorption in and around the NWs. For vertically standing nanowires, the waveguiding effect plays a critical role. The NWs support various resonant waveguide modes which can be excited under the normal incidence of the pump light, and thus the absorption characteristics of the NWs are mainly determined by the excitation of resonant waveguide modes supported by the NWs. Furthermore, under the current configuration, only HE_{1n} modes can be excited, in

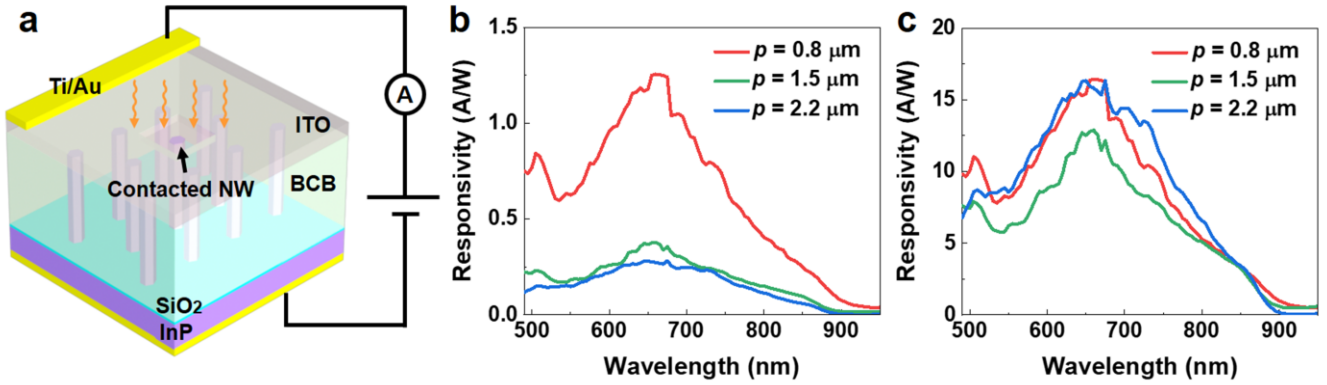

Figure 6. (a) Schematic of single vertical NW photodetector standing in an array. Photoresponse spectrum of (b) unit cell and (c) single NW of as fabricated single vertical NW photodetector from the array with period of 0.8, 1.5 and 2.2 μm, respectively.

which the NW efficiency is determined by how strongly the fields are confined to the NW.[37] A detailed investigation on the absorption spectral feature with increasing nanowire radius can be seen in Section 6 of Supporting Information. The influence of the NW shape on the light localization and confinement in the NWs has also been studied, as shown in Section 7 of Supporting Information. We found that with the standard hexagonal shape, the NW absorptance could reach a maximum value near 100% when compared with irregular hexagonal shapes, further highlighting the advantage of arrays with an optimal pitch size (0.8 μm in this case) and regular hexagonal shape that provides high absorption per unit area.

To evaluate the device performance of as-fabricated single vertical NW photodetectors in Figure 6 (a), the spectral responsivity (R) of the NW from the array was obtained by the following equation: [5, 51]

$$R = \frac{I_{\mathrm{ph}}}{P_{\mathrm{in}}}, \tag{3}$$

where I_{ph} is the photocurrent and P_{in} is the light power incident onto the pitch area (p^2), which enables the direct comparison of the NW array device performance with its planar equivalent while much-reduced material is used. As shown in Figure 6 (b), the responsivity for the NW array with a pitch of 0.8 μm at the peak wavelength of 660 nm and a bias voltage of 1 V is 1.26 A/W, corresponding to the external quantum efficiency ($EQE = \frac{hc}{q\lambda}R \times 100\%$)[52] of 2.37 ×10^2%, where h is the Planck's constant, c is the speed of

light, q is the elementary charge, and λ is the wavelength of incident light. It indicates the strong resonance and thus enhanced absorption in vertical NWs due to the coupling of incident light to HE_{12} guided modes. So far, there is no report on InP NW array photoconductors and our detector has shown good performance comparable to or even better than other reported III-V NW array photodetectors.[53] The absorption branch due to the in-coupling of light into HE_{13} guided mode is also visible but at a much lower magnitude as indicated by the resonance at 505 nm. The cutoff tail from 850 to 900 nm corresponds well to the band edge absorption, as indicated by PL spectrum in Figure 1 (g). When the pitch size is increased from 0.8 to 2.2 μm, the responsivity decreases gradually, consistent with the trend of simulated absorptance as shown in Figure 5 (a) and (c). If P_{in} is assumed as the light power incident onto the physical cross-section of each NW, the responsivity and EQE of the single NW in array with p = 0.8 μm at 660 nm and 1 V is calculated to be 16.45 A/W and 3.10×10^3%, respectively, much larger than the values obtained from of our single horizontal InP NW photodetectors (0.39 A/W and 73.41%) measured at similar conditions.[27] High responsivity per NW from all three arrays as shown in Figure 6 (c) is consistent with the simulated high absorption efficiency of vertical NWs as shown in Figure 5 (b) and (c), confirming the high light concentration in vertical configuration based NWs as well as strong light interaction in small pitch NW arrays that could also help with the absorption boost.

Conclusions

In summary, in this work we developed a FIB based technique to fabricate single vertical InP NW photodetectors in ordered NW arrays grown by SA-MOVPE. By employing a scanning photocurrent imaging technique and FDTD simulation, we thoroughly studied the photocurrent generation from single vertical InP NW photodetectors to unveil light-matter interaction of single vertical NWs standing in an ordered nanowire array. It is shown that light absorption strongly depends on the array pitch size and NW geometry. A significantly high light absorption was observed in single vertical NW photodetectors due to the vertical configuration that results in a resonant increase in the absorption cross-section. It is also

discovered that although the absorption cross-section and thus built-in light concentration is much enhanced for NWs from larger pitch arrays, the maximum absorption efficiency of single NWs from arrays and thus the photodetector performance is obtained by an optimal trade-off between vertical configuration-introduced large absorption cross-section and strong light interaction among NWs in the array. Based on our technique, a high responsivity and external quantum efficiency of 1.26 A/W and 2.37 $\times 10^2$% were obtained for the NW array with a pitch of 0.8 μm (@660 nm, 1 V), indicating good performance of our NW array photodetector device. Our study provides a new approach to study the fundamental optical properties of both single NWs and NW arrays for optoelectronic applications.

Author contributions

L. F. and Z.Y. L. contributed the central idea. Z.Y. L. did the main contribution to the work including the device fabrication, characterization and simulation, and wrote the initial draft of the paper. L. L did the focused ion beam milling, F. W. initiated the Matlab code for the deconvolution of mappings, L. X. did the Lumerical simulations and analysis, Q. G. did the nanowire growth, A. A., K. P. and K. V. assisted with the device fabrication. H. T. H. assisted with FullWAVE simulations. All the authors contributed to refining the ideas and finalizing this paper.

Conflicts of interest

There are no conflicts to declare.

Acknowledgments

The authors would like to acknowledge the financial support from the Australian Research Council (ARC) and facility support from the Australian National Fabrication Facility (ANFF) ACT node. The assistance of resources and services from the National Computational Infrastructure (NCI) is also acknowledged.

References

1. E. Lai, W. Kim and P. Yang, *Nano Res.*, 2008, **1**, 123-128.
2. S. Maeda, K. Tomioka, S. Hara and J. Motohisa, *Jpn. J. Appl. Phys.*, 2012, **51**, 02BN03.
3. I. Yang, S. Kim, M. Niihori, A. Alabadla, Z. Li, L. Li, M. N. Lockrey, D.-Y. Choi, I. Aharonovich, J. Wong-Leung, H. H. Tan, C. Jagadish and L. Fu, *Nano Energy*, 2020, **71**, 104576.
4. T. Frost, S. Jahangir, E. Stark, S. Deshpande, A. Hazari, C. Zhao, B. S. Ooi and P. Bhattacharya, *Nano Lett.*, 2014, **14**, 4535-4541.
5. K. Li, X. Liu, Q. Wang, S. Zhao and Z. Mi, *Nat. Nanotechnol.*, 2015, **10**, 140-144.
6. J. Wallentin, N. Anttu, D. Asoli, M. Huffman, I. Åberg, M. H. Magnusson, G. Siefer, P. Fuss-Kailuweit, F. Dimroth and B. Witzigmann, *Science*, 2013, **339**, 1057-1060.
7. M. Yao, N. Huang, S. Cong, C.-Y. Chi, M. A. Seyedi, Y.-T. Lin, Y. Cao, M. L. Povinelli, P. D. Dapkus and C. Zhou, *Nano Lett.*, 2014, **14**, 3293-3303.
8. Q. Gao, Z. Li, L. Li, K. Vora, Z. Li, A. Alabadla, F. Wang, Y. Guo, K. Peng, Y. C. Wenas, S. Mokkapati, F. Karouta, H. H. Tan, C. Jagadish and L. Fu, *Prog. Photovoltaics Res. Appl.*, 2019, **27**, 237-244.
9. H. W. Shin, S. J. Lee, D. G. Kim, M.-H. Bae, J. Heo, K. J. Choi, W. J. Choi, J.-w. Choe and J. C. Shin, *Sci. Rep.*, 2015, **5**, 10764.
10. S. J. Gibson, B. van Kasteren, B. Tekcan, Y. Cui, D. van Dam, J. E. M. Haverkort, E. P. A. M. Bakkers and M. E. Reimer, *Nat. Nanotechnol.*, 2019, **14**, 473-479.
11. H. Jeddi, M. Karimi, B. Witzigmann, X. Zeng, L. Hrachowina, M. T. Borgström and H. Pettersson, *Nanoscale*, 2021, **13**, 6227-6233.
12. Z. Li, S. Trendafilov, F. Zhang, M. S. Allen, J. W. Allen, S. U. Dev, W. Pan, Y. Yu, Q. Gao, X. Yuan, I. Yang, Y. Zhu, A. Bhat, S. X. Peng, W. Lei, H. H. Tan, C. Jagadish and L. Fu, *Nano Lett.*, 2021, **21**, 7388-7395.
13. Y. Lu, S. Peng, D. Luo and A. Lal, *Nat. Commun.*, 2011, **2**, 578.
14. K. R. Rostgaard, R. S. Frederiksen, Y.-C. C. Liu, T. Berthing, M. H. Madsen, J. Holm, J. Nygård and K. L. Martinez, *Nanoscale*, 2013, **5**, 10226-10235.
15. A. Convertino, V. Mussi and L. Maiolo, *Sci. Rep.*, 2016, **6**, 25099.
16. Z. Li, H. H. Tan, C. Jagadish and L. Fu, *Advanced Materials Technologies*, 2018, **3**, 1800005.
17. X. Yuan, D. Pan, Y. Zhou, X. Zhang, K. Peng, B. Zhao, M. Deng, J. He, H. H. Tan and C. Jagadish, *Applied Physics Reviews*, 2021, **8**, 021302.
18. L. C. Chuang, M. Moewe, C. Chase, N. P. Kobayashi, C. Chang-Hasnain and S. Crankshaw, *Appl. Phys. Lett.*, 2007, **90**, 043115.
19. K. Tomioka, J. Motohisa, S. Hara, K. Hiruma and T. Fukui, *Nano Lett.*, 2010, **10**, 1639-1644.
20. M. Heurlin, P. Wickert, S. Fält, M. T. Borgström, K. Deppert, L. Samuelson and M. H. Magnusson, *Nano Lett.*, 2011, **11**, 2028-2031.
21. L. Tsakalakos, J. Balch, J. Fronheiser, M.-Y. Shih, S. F. LeBoeuf, M. Pietrzykowski, P. J. Codella, B. A. Korevaar, O. Sulima and J. Rand, *J. Nanophotonics*, 2007, **1**, 013552.
22. S. L. Diedenhofen, O. T. Janssen, G. Grzela, E. P. Bakkers and J. Gómez Rivas, *ACS Nano*, 2011, **5**, 2316-2323.
23. B. M. Kayes, H. A. Atwater and N. S. Lewis, *J. Appl. Phys.*, 2005, **97**, 114302.
24. Z. Fan, H. Razavi, J.-w. Do, A. Moriwaki, O. Ergen, Y.-L. Chueh, P. W. Leu, J. C. Ho, T. Takahashi and L. A. Reichertz, *Nat. Mater.*, 2009, **8**, 648-653.
25. J. M. Spurgeon, S. W. Boettcher, M. D. Kelzenberg, B. S. Brunschwig, H. A. Atwater and N. S. Lewis, *Adv. Mater.*, 2010, **22**, 3277-3281.
26. Q. Gao, D. Saxena, F. Wang, L. Fu, S. Mokkapati, Y. Guo, L. Li, J. Wong-Leung, P. Caroff, H. H. Tan and C. Jagadish, *Nano Lett.*, 2014, **14**, 5206-5211.

27. K. Peng, P. Parkinson, J. L. Boland, Q. Gao, Y. C. Wenas, C. L. Davies, Z. Li, L. Fu, M. B. Johnston, H. H. Tan and C. Jagadish, *Nano Lett.*, 2016, **16**, 4925-4931.
28. P. Krogstrup, H. I. Jørgensen, M. Heiss, O. Demichel, J. V. Holm, M. Aagesen, J. Nygard and A. F. i Morral, *Nat. Photonics*, 2013, **7**, 306-310.
29. D. van Dam, N. J. van Hoof, Y. Cui, P. J. van Veldhoven, E. P. Bakkers, J. Gómez Rivas and J. E. Haverkort, *ACS Nano*, 2016, **10**, 11414-11419.
30. V. Raj, T. S. Dos Santos, F. Rougieux, K. Vora, M. Lysevych, L. Fu, S. Mokkapati, H. H. Tan and C. Jagadish, *J. Phys. D Appl. Phys.*, 2018, **51**, 395301.
31. J. Meng, J. J. Cadusch and K. B. Crozier, *Nano Lett.*, 2019, **20**, 320-328.
32. S. Mauthe, Y. Baumgartner, M. Sousa, Q. Ding, M. D. Rossell, A. Schenk, L. Czornomaz and K. E. Moselund, *Nat. Commun.*, 2020, **11**, 4565.
33. F. Wang, Q. Gao, K. Peng, Z. Li, Z. Li, Y. Guo, L. Fu, L. M. Smith, H. H. Tan and C. Jagadish, *Nano Lett.*, 2015, **15**, 3017-3023.
34. Z. Zhong, Z. Li, Q. Gao, Z. Li, K. Peng, L. Li, S. Mokkapati, K. Vora, J. Wu, G. Zhang, Z. Wang, L. Fu, H. H. Tan and C. Jagadish, *Nano Energy*, 2016, **28**, 106-114.
35. Z. Li, I. Yang, L. Li, Q. Gao, J. S. Chong, Z. Li, M. N. Lockrey, H. H. Tan, C. Jagadish and L. Fu, *Prog. Nat. Sci.: Mater. Int.*, 2018, **28**, 178-182.
36. Z. Li, Y. C. Wenas, L. Fu, S. Mokkapati, H. H. Tan and C. Jagadish, *IEEE J. Photovolt.*, 2015, **5**, 854-864.
37. S. Mokkapati, D. Saxena, H. H. Tan and C. Jagadish, *Sci. Rep.*, 2015, **5**.
38. N. Anttu and H. Xu, *Opt. Express*, 2013, **21**, A558-A575.
39. A. Nowzari, M. Heurlin, V. Jain, K. Storm, A. Hosseinnia, N. Anttu, M. T. Borgström, H. k. Pettersson and L. Samuelson, *Nano Lett.*, 2015, **15**, 1809-1814.
40. N. Anttu, *Nanotechnology*, 2019, **30**, 104004.
41. N. Anttu, A. Abrand, D. Asoli, M. Heurlin, I. Åberg, L. Samuelson and M. Borgström, *Nano Res.*, 2014, **7**, 816-823.
42. R. Frederiksen, G. Tutuncuoglu, F. Matteini, K. L. Martinez, A. F. i Morral and E. Alarcon-Llado, *ACS Photonics*, 2017, **4**, 2235.
43. G. Otnes, E. Barrigón, C. Sundvall, K. E. Svensson, M. Heurlin, G. Siefer, L. Samuelson, I. Åberg and M. T. Borgström, *Nano Lett.*, 2018, **18**, 3038-3046.
44. E. Barrigón, L. Hrachowina and M. T. Borgström, *Nano Energy*, 2020, **78**, 105191.
45. Q. Gao, PhD, The Australian National University, 2016.
46. Z. Fan, P.-c. Chang, J. G. Lu, E. C. Walter, R. M. Penner, C.-h. Lin and H. P. Lee, *Appl. Phys. Lett.*, 2004, **85**, 6128-6130.
47. H. Kind, H. Yan, B. Messer, M. Law and P. Yang, *Adv. Mater.*, 2002, **14**, 158.
48. S.-C. Kung, W. Xing, W. E. van der Veer, F. Yang, K. C. Donavan, M. Cheng, J. C. Hemminger and R. M. Penner, *ACS Nano*, 2011, **5**, 7627-7639.
49. Y. Jiang, W. J. Zhang, J. S. Jie, X. M. Meng, X. Fan and S. T. Lee, *Adv. Funct. Mater.*, 2007, **17**, 1795-1800.
50. Z. Li, H. T. Hattori, L. Fu, H. H. Tan and C. Jagadish, *J. Light. Technol*, 2011, **29**, 2690-2697.
51. L. Ma, W. Hu, Q. Zhang, P. Ren, X. Zhuang, H. Zhou, J. Xu, H. Li, Z. Shan, X. Wang, L. Liao, H. Q. Xu and A. Pan, *Nano Lett.*, 2014, **14**, 694-698.
52. J. Liu, F. Liu, H. Liu, J. Yue, J. Jin, J. Impundu, H. Liu, Z. Yang, Z. Peng, H. Wei, C. Jiang, Y. J. Li, L. Xie and L. Sun, *Nano Today*, 2021, **36**, 101055.
53. R. R. LaPierre, M. Robson, K. M. Azizur-Rahman and P. Kuyanov, *J. Phys. D Appl. Phys.*, 2017, **50**, 123001.